Distorted-wave cross sections for electron-impact ionization of Ar^{7+}

K. J. Reed and M. H. Chen
Atomic Processes Group, Lawrence Livermore National Laboratory, Livermore, California 94550
(Received 27 February 1996)

Distorted-wave methods have been used to calculate cross sections for electron-impact ionization of sodiumlike Ar^{7+} for collision energies ranging from near threshold to 1 keV. We included contributions due to excitation-autoionization and resonant excitation–double autoionization (REDA), as well as the contributions from direct ionization of the $3s$ electron and the $n=2$ inner-shell electrons. We find that the effects of radiative damping and loss channels reduce the REDA contributions by a factor of 4. We compare our calculated results to experimental results and to theoretical cross sections obtained in a close-coupling approximation. [S1050-2947(96)09009-9]

PACS number(s): 34.80.Kw

I. INTRODUCTION

In this paper we discuss distorted-wave calculations of cross sections for electron-impact ionization of sodiumlike argon. Theoretical and experimental investigations have demonstrated that electron-impact ionization of positive ions can be dominated by indirect processes which often make greater contributions to the total ionization cross section than does the process of direct ionization [1–10]. Excitation-autoionization and resonant excitation–double autoionization (REDA) are the most important of these indirect processes. In excitation autoionization, the incident electron excites an inner-shell electron leaving the target ion in an excited state which can decay by autoionization. The REDA process occurs when the incident electron excites an inner-shell electron and is simultaneously captured by the target ion, resulting in a doubly excited state which decays by two sequential Auger processes. The REDA process was postulated in 1981 by LaGatutta and Hahn [10]. While excitation-autoionization processes are frequently included in calculations of electron-impact ionization of positive ions, the REDA processes have usually been neglected because of their complexity. Most of the calculations which include REDA have been performed for ions in the Li-like [11–16] and Na-like [17–21] isoelectronic sequences because of the relatively simple atomic structure of these ions. Calculations of REDA contributions to ionization of some Be-like and B-like ions [16] and Mg-like Xe^{42+} [19] have also been reported.

In our previous studies of excitation-autoionization contributions to electron-impact ionization of Na-like ions with $26 \leqslant Z \leqslant 92$, we found that excitation-autoionization processes generally enhance the ionization cross sections by about a factor of 4 for these ions [21]. Experiments using the electron-beam ion trap at LLNL verified this excitation-autoionization enhancement for Xe^{43+} [23]. Our theoretical studies of Fe^{15+} [16], Kr^{25+}, and Xe^{43+} [20] showed that the REDA processes produced numerous strong resonances which contributed as much as 15% to 30% to the average ionization cross sections for these sodiumlike ions. Measurements made at the Test Storage Ring in Germany have confirmed our calculations of the REDA resonances in Fe^{15+} and demonstrated similar resonance structure in the cross sections for Se^{23+} [24]. We have also rececently reported similar theoretical results for REDA contributions to ionization of Se^{23+} [25]. From our earlier studies of REDA in Li- and Na-like ions, we note that the importance of the REDA contributions relative to the direct ionization cross sections generally increases with increasing charge state in these isoelectronic sequences. This is partly because the direct ionization cross sections rapidly decrease with increasing charge state. However, for very high-Z ions this trend is offset by the radiative decay rates, which increase approximately as Z^4. Consequently, the REDA contributions for high-Z ions such as Au^{68+} [17] are much less significant than the REDA contributions mentioned above for Fe^{15+} or Se^{23+}.

Experimental measurements of cross sections for electron-impact ionization of Ar^{7+} have been reported by Rachafi *et al.* [26] and by Zhang *et al.* [27]. The results reported from these two experiments differ substantially from each other at incident electron energies greater than 350 eV. In addition, a close-coupling calculation of electron-impact ionization cross sections for Ar^{7+} has recently been performed by Tayal [28]. The theoretical results we report here were obtained using distorted-wave methods. Distorted-wave electron-impact ionization cross sections for Ar^{7+} including excitation autoionization previously calculated by Griffin *et al.* were shown in Ref. [27]. However, these calculations did not include the REDA contribution or the contributions of direct ionization of the $n=2$ inner-shell electrons.

II. CALCULATIONAL PROCEDURE

Our theoretical approach has been described in detail previously [16,17]. We carried out separate fully relativistic calculations for the direct ionization cross sections, the cross sections for excitation to the intermediate autoionizing states, and the radiative and Auger rates for decay of the autoionizing states. The processes considered in this work are shown schematically below:

$$e+1s^2 2l^8 3s \rightarrow 1s^2 2l^8 + e + e, \tag{1}$$

$$e+1s^2 2l^8 3s \rightarrow 1s^2 2l^7 3s + e + e, \tag{2}$$

$$e+1s^2 2l^8 3s \rightarrow 1s^2 2l^7 3snl(n=3-6) + e \rightarrow 1s^2 2l^8 + e + e, \tag{3}$$

$$e+1s^2 2l^8 3s \rightarrow 1s^2 2l^7 3p^2 + e \rightarrow 1s^2 2l^8 + e + e, \quad (4)$$

and

$$e+1s^2 2l^8 3s \rightarrow 1s^2 2l^7 3snln'l' \rightarrow 1s^2 2l^7 3sn''l'' + e \rightarrow 1s^2 2l^8 + e + e. \quad (5)$$

As indicated in Eqs. (1) and (2), we included direct ionization of the inner-shell $n=2$ electrons as well as direct ionization of the $3s$ electron. The excitation-autoionization processes included are indicated in Eqs. (3) and (4). We carried out detailed calculations of excitation cross sections for the intermediate autoionizing states with $n=3$, and we used a configuration-average approximation to obtain cross sections for exciting the intermediate states with $n=4$ to 6.

The direct ionization, excitation-autoionization, and REDA processes are assumed to be independent. In this approximation the total ionization cross section σ_t is given by

$$\sigma_t = \sigma_d + \sum_i \sigma_i^{\rm ex} B_i^A + \sum_k \overline{\sigma}_k^{\rm cap} B_k^{dA}. \quad (6)$$

Here, σ_d is the direct ionization cross section, which is the sum of the cross sections for direct ionization of the $n=2$ electrons and the $3s$ electron. $\sigma_i^{\rm ex}$ and $\overline{\sigma}_k^{\rm cap}$ are excitation and energy-averaged dielectronic capture cross sections, respectively; B_i^A and B_k^{dA} are the branching ratios for the single and sequential double Auger emission, respectively.

The single and double Auger branching ratios can be written as

$$B_i^A = \frac{\Sigma_{j_f} A_{ij}^A}{\Sigma_m A_{im}^A + \Sigma_k A_{ik}^r}, \quad (7)$$

and

$$B_k^{dA} = \frac{\sum_{k'} A_{kk'}^A \sum_f A_{k'f}^A}{\left(\sum_m A_{km}^A + \sum_n A_{kn}^r\right)\left(\sum_m A_{k'm}^A + \sum_n A_{k'n}^r\right)}, \quad (8)$$

where A_{ij}^A and A_{ik}^r are the Auger and radiative transition rates, respectively.

The energy-averaged capture cross section from the initial state i to the intermediate-state k in cm^2 is obtained from the inverse Auger process by detail balance [10]:

$$\overline{\sigma}_k^{\rm cap} = \frac{4.95\times 10^{-30}}{\Delta E E_k} \frac{g_k}{2g_i} A_{ki}^A. \quad (9)$$

Here ΔE and E_k are the energy bin and Auger energy in eV; g_k and g_i are the statistical weights and the Auger rate is in units of sec^{-1}.

The direct ionization cross sections [Eqs. (1) and (2)] were obtained using a code developed by Zhang and Sampson [29]. The detailed cross sections for excitation to the $n=3$ intermediate autoionizing states were calculated using a relativistic distorted-wave method [30], and the configuration-averaged cross sections for excitation to the $n=4$, 5, and 6 intermediate states were calculated using a separate relativistic distorted-wave excitation code [31]. The capture cross sections [Eq. (9)], and the single Auger [Eq. (7)] and double Auger [Eq. (8)] branching ratios were evaluated using the multiconfiguration Dirac-Fock (MCDF) model [32,33] in intermediate coupling with configuration interaction from the same complex. For those intermediate states in Eq. (3) with $n=4$ to 6, we assumed unit branching ratios.

For the REDA ionizing process [Eq. (5)], we carried out explicit calculations for resonant states from $2s^2 2p^5 3s4lnl'$ ($n=4-8$, $l' \leq 4$), $2s2p^6 3s4lnl'$ ($n=4-8$, $l' \leq 4$), $2s^2 2p^5 3s3lnl'$ ($n=6-10$, $l' \leq 6$), and $2s2p^6 3s3lnl'$ ($n=6-10$, $l' \leq 6$). Extrapolation to $n=50$ was accomplished using the n^{-3} scaling law for the Auger transition rates. The Auger branching ratios were calculated by including all possible Auger channels and electric-dipole decays with change of principal quantum number (i.e., $\Delta n \neq 0$). The total cross sections were computed according to Eq. (6) by summing the direct, excitation-autoionization, and REDA cross sections.

TABLE I. Energy levels, branching ratios (B^A), and excitation-autoionization cross sections for some intermediate states in Ar^{7+} at incident electron energy of 385 eV. The number in brackets denotes the power of 10.

Level	Energy (eV)	Configuration	B^A	Cross Section (cm^2)
6	246.60	$(2p_{3/2}3s^2)_{3/2}$	0.937	1.65 [−20]
7	248.83	$(2p_{1/2}3s^2)_{1/2}$	0.937	7.51 [−20]
10	260.38	$(2p_{3/2}3s3p_{1/2})_{5/2}$	0.008	9.52 [−23]
11	260.74	$(2p_{3/2}3s3p_{1/2})_{3/2}$	0.030	2.36 [−22]
17	263.32	$(2p_{1/2}3s3p_{1/2})_{1/2}$	0.188	7.88 [−22]
20	264.60	$(2p_{1/2}3s3p_{3/2})_{1/2}$	0.912	1.70 [−20]
22	269.23	$(2p_{3/2}3s3p_{3/2})_{3/2}$	0.780	4.97 [−21]
24	271.01	$(2p_{1/2}3s3p_{3/2})_{1/2}$	0.986	1.28 [−20]
43	286.17	$(2p_{3/2}3s3d_{3/2})_{1/2}$	0.873	1.01 [−20]
44	286.41	$(2p_{3/2}3s3d_{3/2})_{3/2}$	0.865	1.64 [−20]
48	287.46	$(2p_{3/2}3s3d_{5/2})_{7/2}$	0.587	8.55 [−22]
51	288.31	$(2p_{3/2}3s3d_{5/2})_{3/2}$	0.154	1.09 [−21]
54	289.38	$(2p_{3/2}3s3d_{3/2})_{1/2}$	0.966	5.31 [−20]
55	289.53	$(2p_{3/2}3s3d_{5/2})_{3/2}$	0.953	2.93 [−20]
58	290.78	$(2p_{1/2}3s3d_{3/2})_{3/2}$	0.999	1.18 [−20]
62	292.82	$(2p_{3/2}3s3d_{3/2})_{3/2}$	0.993	2.67 [−19]
63	292.82	$(2p_{3/2}3s3d_{5/2})_{3/2}$	0.994	1.95 [−20]
64	294.68	$(2p_{3/2}3s3d_{5/2})_{7/2}$	0.987	1.48 [−20]
66	296.35	$(2p_{3/2}3s3d_{5/2})_{3/2}$	0.982	6.94 [−20]
67	296.67	$(2p_{3/2}3s3d_{5/2})_{1/2}$	0.973	7.04 [−20]
69	298.46	$(2p_{1/2}3s3d_{3/2})_{3/2}$	0.981	1.04 [−19]
135	325.67	$(2s3s^2)_{1/2}$	1.000	5.49 [−20]
179	337.81	$(2s3s3p_{1/2})_{1/2}$	0.946	2.02 [−21]
181	338.23	$(2s3s3p_{3/2})_{5/2}$	0.155	7.86 [−22]
187	347.45	$(2s3s3p_{3/2})_{3/2}$	0.999	1.58 [−22]
197	365.01	$(2s3s3d_{3/2})_{5/2}$	1.000	1.00 [−20]
198	365.02	$(2s3s3d_{5/2})_{7/2}$	1.000	1.36 [−20]
202	373.43	$(2s3s3d_{5/2})_{5/2}$	0.999	1.31 [−20]

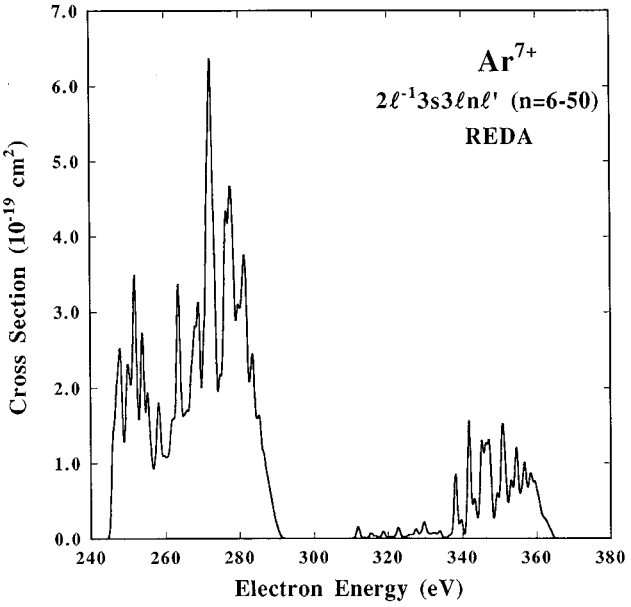

FIG. 1. REDA cross sections for the $2l^{-1}3s3lnl'$ (n=6–50) as a function of impact electron energy.

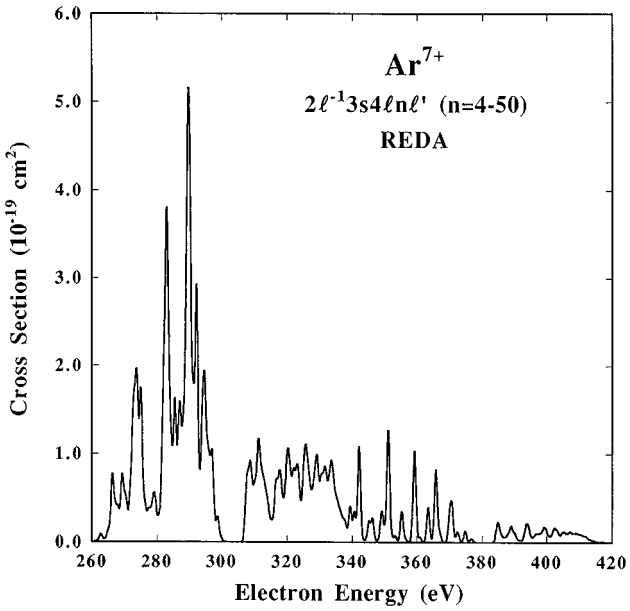

FIG. 2. REDA cross sections for the $2l^{-1}3s4l4l'$ (n=4–50) as a function of impact electron energy.

III. RESULTS AND DISCUSSION

In Table I we list the excitation energies, the branching ratios, and the excitation-autoionization cross sections for some of the important intermediate autoionizing states of Ar^{7+}. The excitation-autoionization cross section for a state is the product of the excitation cross section and the branching ratio for that state. The level indices refer to the ordering of all of the states in the atomic-structure calculation for the target Ar^{7+} ion. In our configuration notation, the first orbital in the configuration is the inner shell having a vacancy. The last two orbitals give the outer-shell occupations. The subscript outside the parentheses gives the total angular momentum for the state. The cross sections listed in the table are at an incident electron energy of 385 eV where all of the channels for the $n=2$ to $n=3$ excitations are open. Most of the branching ratios are near unity, but there is some variation. At 385 eV, radiative damping decreases the total excitation-autoionization contribution by about 13%.

The $(2p_{3/2}3s^2)_{3/2}$ state (level 6) and the $(2p_{1/2}3s^2)_{1/2}$ state (level 7) both have very large excitation-autoionization cross sections, and the combined contributions from these two intermediate states produce a large abrupt increase in the ionization cross section near 250 eV. The two largest contributions are from the $(2p_{3/2}3s3d_{3/2})_{3/2}$ state (level 62) and the $(2p_{1/2}3s3d_{3/2})_{3/2}$ state (level 69), respectively. The excitation-autoionization processes due to the $n=2$ to $n=3$ excitations enhance the direct ionization cross section by about a factor of 4, consistent with the enhancement we found previously for other Na-like ions [22]. The threshold for the $n=2$ to $n=4$ excitations is around 325 eV.

The REDA cross sections for the $2l^{-1}3s3lnl'$ (n=6–50) and the $2l^{-1}3s4l4l'$ (n=4–50) intermediate autoionizing states are shown in Figs. 1 and 2, respectively. The effect of radiative decay on the REDA cross sections can be seen in Figs. 3 and 4. Radiative decay reduces the cross sections for the $3l6l'$ and $4l4l'$ intermediate states by as much as a factor of 2.5. While this is not as dramatic as the effect of radiative decay, we noted that for the REDA cross sections for higher-Z sodiumlike ions, it is nevertheless a substantial decrease in the contribution that these states make to the ionization cross section for Ar^{7+}.

In addition to the decrease caused by radiative damping,

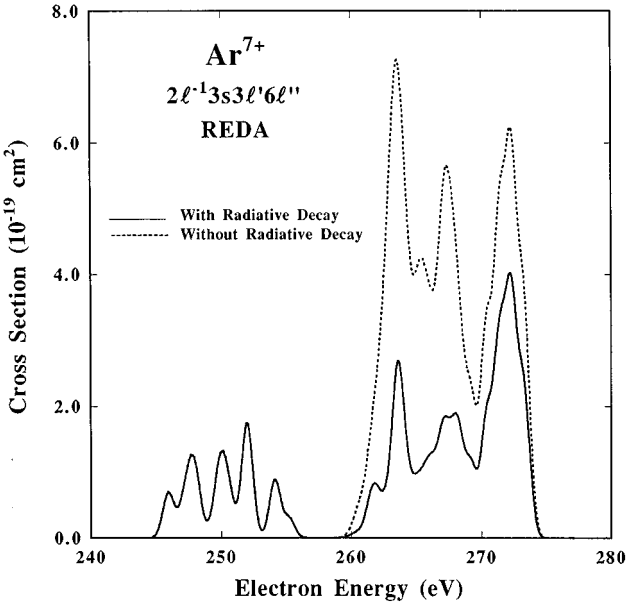

FIG. 3. REDA cross sections for the $2l^{-1}3s3lnl'$ (n=6–50) as a function of impact electron energy. The dotted curve shows the cross sections without radiative damping. The solid curve shows the cross sections with radiative damping included.

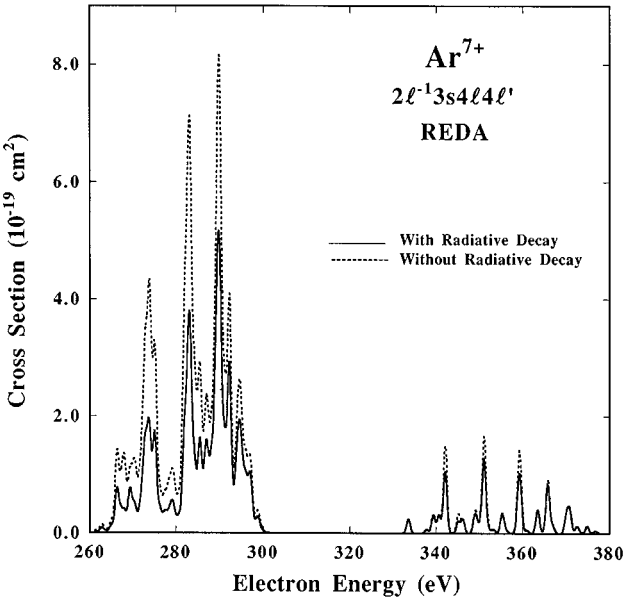

FIG. 4. REDA cross sections for the $2l^{-1}3s4l4l'$ ($n=4$–50) as a function of impact electron energy. The legend is the same as in Fig. 3.

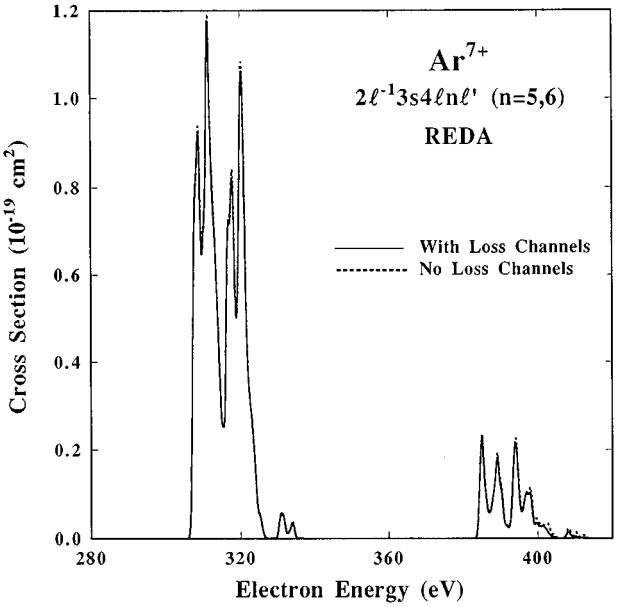

FIG. 5. The effects of loss channels on the REDA cross sections for the $2l^{-1}3s4lnl'$ ($n=5,6$) intermediate states. The dotted curve shows the cross sections without the effects of loss channels. The solid curve shows the cross sections calculated with the loss channels included.

there is a further reduction in the REDA cross sections due to the effect of channels known as loss channels. To explain the process which produces these loss channels we refer to Eq. (5). The first step of Eq. (5) shows the formation of a doubly excited Mg-like intermediate state which decays to an autoionizing state of Na-like argon. However, the Mg-like intermediate state can also decay to an excited bound state of Ar^{7+} as in Eq. (10),

$$e+1s^2 2l^8 3s \rightarrow 1s^2 2l^7 3snl'n''l'' \rightarrow 1s^2 2l^8 n''l''+e. \tag{10}$$

The excited bound state stabilizes by radiative decay so the process does not contribute to the cross section for ionization of the sodiumlike ion, and thus represents a loss to the ionization channels. In Fig. 5 it can be seen that the effect of loss channels on the $2l^{-1}3s4lnl'$ ($n=5,6$) REDA resonances is essentially negligible. But Fig. 6 shows that the loss channels reduce the $2l^{-1}3s3lnl'$ ($n=6$–10) REDA cross sections by as much as a factor of 3.

Our calculated results are shown in Fig. 7, along with the experimental cross sections reported by Rachafi *et al.* [26] and the results obtained in crossed-beam experiments by Zhang *et al.* [27]. The threshold for direct ionization of the $n=2$ inner-shell electrons is about 394 eV and this process produces the sudden rise in the decreasing direct ionization cross section near this energy in Fig. 7.

Above 375 eV the two sets of experimental cross sections differ markedly from each other. In this region the close-coupling results reported by Tayal [28] fall about midway between the two sets of experimental data. However, our calculated results in this region are larger than those reported by Tayal, and are in very good agreement with the crossed-beam results reported by Zhang *et al.* The close-coupling calculations reported by Tayal included autoionizing states arising from $1s^2 2l^7 3snl$ configurations with $n=3$ and 4. In our calculations we included those same configurations, but also added states having $n=5$ and 6. The differences in magnitude between our results and those of Tayal in this energy region arise from the contributions of these additional intermediate states with $n=5$ and 6. When we restrict our calcu-

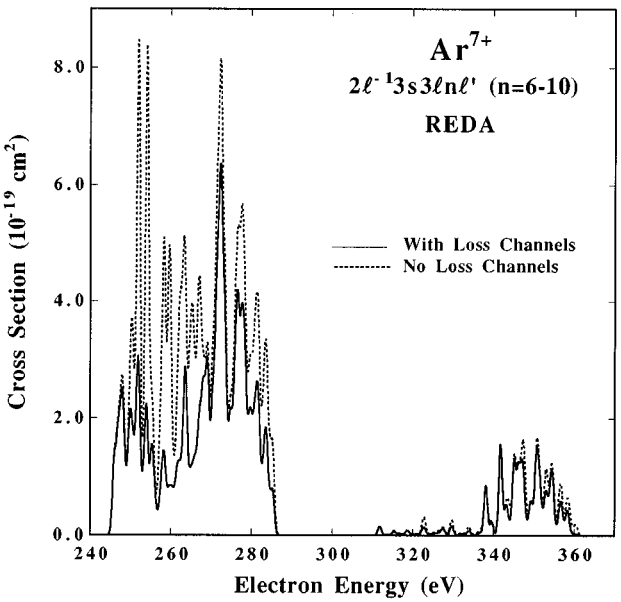

FIG. 6. The effects of loss channels on the REDA cross sections for the $2l^{-1}3s3lnl'$ ($n=6$-10) intermediate states. The legend is the same as in Fig. 5.

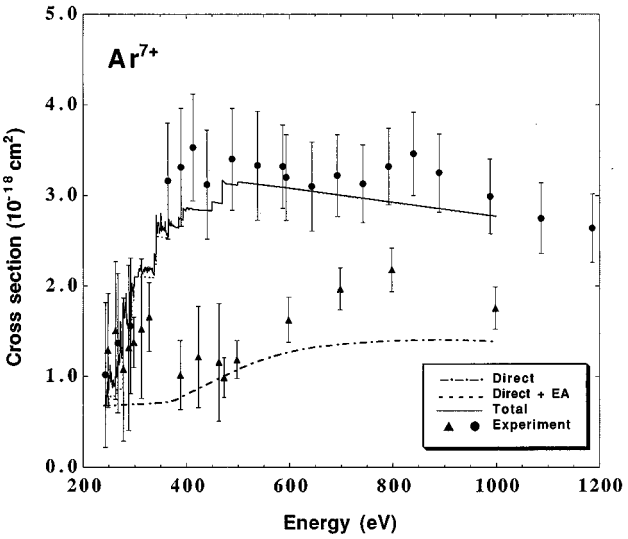

FIG. 7. Cross sections for Ar^{7+} as functions of incident electron energy. The dashed curve shows the direct ionization cross sections. The dotted curve is the sum of the direct ionization and the excitation-autoionization cross sections. The solid curve shows the calculated total cross sections. The triangles are the experimental results reported by Rachafi *et al.* [26], and the solid circles show the experimental results reported by Zhang *et al.* [27].

lations to configurations with $n \leqslant 4$, our results in this region are close to the results reported by Tayal.

In the energy region below 375 eV there is much better agreement between the two sets of experimental data. This lower-energy region is shown expanded in Fig. 8. In Fig. 8 we also show the close-coupling results reported by Tayal [28]. This energy region is the region where many REDA resonances occur. In this region the REDA resonances in the close-coupling results reported in Ref. [28] are much larger in magnitude than the REDA resonances obtained in our calculations. The differences between our results and the close-coupling results in this region arise from the effects of the loss channels shown in Eq. (10). Singly excited states $1s^2 2l^8 nl$ with $n=3$ and 4 were included in the close-coupling calculation of Ref. [28], but higher excited states with $n>4$ were ignored. However, we found that the states with $5 \leqslant n \leqslant 10$ are also important and including these higher-n excited states reduces the REDA resonances considerably. The experimental data in this region show some fluctuations but are too sparse to map the resonances. However, our calculated cross sections are in good agreement with the experimental data reported in this region.

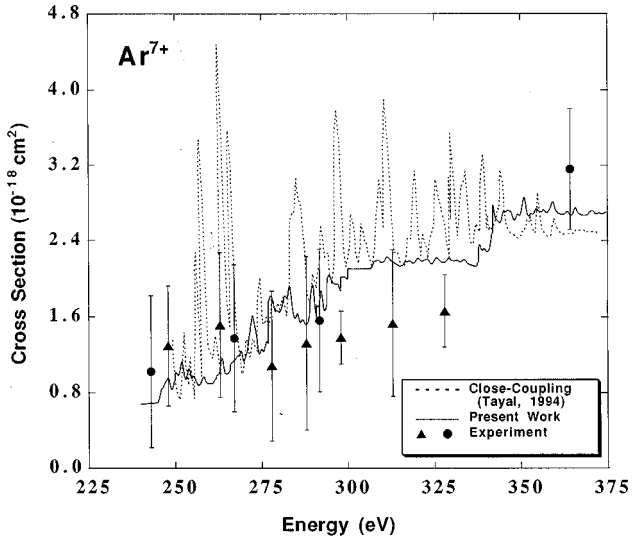

FIG. 8. Comparison of distorted-wave results with close-coupling results and experimental results for Ar^{7+} in the energy region of the REDA resonances. The dotted curve shows the close-coupling cross sections reported by Tayal [16]. The triangles are the experimental results reported by Rachafi *et al.* [20], and the solid circles show the experimental results reported by Zhang *et al.* [21]. The solid line shows the distorted-wave results obtained in the present work.

IV. CONCLUSION

We have carried out distorted-wave calculations for cross sections for electron-impact ionization of sodiumlike Ar^{7+}. These calculations include the effects of excitation autoionization and REDA. We examined the effects of radiative decay on the excitation-autoionization and REDA contributions and the effects of loss channels on the REDA resonances. Despite the reductions caused by radiative decay and loss channels, the indirect processes contribute significantly to the total ionization cross section. We find that these indirect processes significantly enhance the ionization cross sections for this ion. There are important differences between our results and earlier results obtained in a close-coupling calculation. In the region of higher incident electron energy (i.e., above 375 eV) the differences between the two sets of theoretical results can be attributed to contributions from higher-n intermediate autoionizing states which were neglected in the close-coupling calculation. In the lower-energy region where the REDA contributions are important, the differences between results of the two calculations can be attributed to the neglect of higher-n loss channels in the close-coupling calculation, which can result in overestimation of the REDA contribution.

The measured cross sections obtained in two separate experiments differ substantially from each other, especially in the higher-energy region. In the lower-energy region, the two sets of experimental data are closer to each other, and our results in this region are in good agreement with the experimental results reported. The magnitudes of the REDA resonances obtained in the close-coupling calculation are much larger than the experimental cross sections in this region. In the higher-energy region where there are large differences between the experimental results, the close-coupling results are about midway between the two sets of measurements. In this region our results are in very good agreement with the experimental data reported by Zhang *et al.* [27].

ACKNOWLEDGMENT

This work was performed under the auspices of the U.S. Department of Energy by Lawrence Livermore National Laboratory under Contract No. W-7405-ENG-48.

[1] R. A. Falk, G. H. Dunn, D. C. Griffin, C. Bottcher, D. C. Gregory, D. H. Crandall, and M. S. Pindzola, Phys. Rev. Lett. **47**, 494 (1981).
[2] A. Müller and R. Frodl, Phys. Rev. Lett. **44**, 29 (1980).
[3] R. D. Cowan and J. B. Mann, Astrophys. J. **232**, 940 (1979).
[4] R. J. W. Henry and A. Z. Msezane, Phys. Rev. A **26**, 2545 (1982).
[5] M. S. Pindzola and D. C. Griffin, Phys. Rev. A **36**, 2628 (1987).
[6] D. L. Moores and H. Nussbaumer, J. Phys. B **3**, 6 (1970).
[7] D. C. Griffin, C. Bottcher, M. S. Pindzola, S. M. Younger, D. C. Gregory, and D. H. Crandall, Phys. Rev. A **29**, 1729 (1984).
[8] D. H. Crandall, R. A. Phaneuf, R. A. Falk, D. S. Belic, and G. H. Dunn, Phys. Rev. A **25**, 143 (1982).
[9] A. Müller, K. Tinschert, G. Hofman, E. Salzborn, and G. H. Dunn, Phys. Rev. Lett. **61**, 70 (1988); **61**, 1352 (1988).
[10] K. T. LaGatutta and Y. Hahn, Phys. Rev. A **24**, 2273 (1981).
[11] K. J. Reed and M. H. Chen, Phys. Rev. A **45**, 4519 (1992).
[12] M. H. Chen and K. J. Reed, Phys. Rev. A **45**, 4525 (1992).
[13] M. H. Chen and K. J. Reed, Phys. Rev. A **48**, 1129 (1992).
[14] S. S. Tayal and R. J. W. Henry, Phys. Rev. A **42**, 1831 (1990).
[15] S. S. Tayal and R. J. W. Henry, Phys. Rev. A **44**, 2295 (1991).
[16] N. R. Badnell and M. S. Pindzola, Phys. Rev. A **47**, 2937 (1993).
[17] K. J. Reed, M. H. Chen, and D. L. Moores, Phys. Rev. A **41**, 550 (1990).
[18] M. H. Chen, K. J. Reed, and D. L. Moores, Phys. Rev. Lett. **64**, 1350 (1990).
[19] K. J. Reed, M. H. Chen, and D. L. Moores, Phys. Rev. A **42**, 5315 (1990).
[20] M. H. Chen and K. J. Reed, Phys. Rev. A **47**, 1874 (1990).
[21] S. S. Tayal and R. J. W. Henry, Phys. Rev. A **39**, 2295 (1989).
[22] K. J. Reed, M. H. Chen, and D. L. Moores, Phys. Rev. A **44**, 4336 (1991).
[23] D. Schneider, D. DeWitt, M. W. Clark, R. Such, C. L. Cocke, R. Schmieder, K. J. Reed, M. H. Chen, R. E. Marrs, M. Levine, and R. Fortner, Phys. Rev. A **42**, 3889 (1990).
[24] J. Linkmann, A. Müller, J. Kenntner, D. Habs, D. Schwalm, A. Wolf, N. R. Badnell, and M. S. Pindzola, Phys. Rev. Lett. **74**, 4173 (1995).
[25] M. H. Chen and K. J. Reed, Phys. Rev. A **52**, 2881 (1995).
[26] S. Rachafi, D. S. Belic, M. Duponchelle, J. Jureta, M. Zambra, H. Zhang, and P. Defrance, J. Phys. B **24**, 1037 (1991).
[27] Y. Zhang, C. B. Reddy, R. S. Smith, D. E. Golden, and D. W. Muller, Phys. Rev. A **45**, 2929 (1992).
[28] S. S. Tayal, Phys. Rev. A **49**, 2651 (1994).
[29] H. L. Zhang and D. H. Sampson, Phys. Rev. A **42**, 5387 (1990).
[30] P. L. Hagelstein and R. K. Jung, At. Data Nucl. Data Tables **37**, 17 (1987).
[31] D. H. Sampson, H. L. Zhang, A. K. Mohanty, and R. E. H. Clark, Phys. Rev. A **40**, 604 (1989).
[32] M. H. Chen, Phys. Rev. A **31**, 1449 (1985).
[33] I. P. Grant, B. J. McKenzie, P. H. Norrington, D. F. Mayers, and N. C. Pyper, Comput. Phys. Commun. **21**, 207 (1980).